



**AN INVESTIGATION OF FATIGUE CRACK GROWTH
BEHAVIOR OF UIC 54 PROFILE IN HIGH SPEED
RAILWAY APPLICATIONS**

by

**GURUBARAN A/L PANERSELVAN
(1631412061)**

A thesis submitted in fulfillment of the requirements for the degree of
Master of Science in Mechanical Engineering

**School of Mechatronic Engineering
UNIVERSITI MALAYSIA PERLIS
2017**

ACKNOWLEDGMENT

First and foremost, I would like to thank the Almighty God for all the will power, strength and unfailing love given to me to complete this study. My deepest appreciation and a million thanks to my dedicated project supervisor Dr. Mohd Afendi Bin Rojan for giving me his previous time and thoughtful encouragement to complete the research.

Apart from that, I have gained heaps of knowledge and skill of teamwork to solve some engineering problems regarding research. I also would like to thank all Universiti Malaysia Perlis lecturers, especially former senior lecturer Dr. Haftirman Idrus, teaching engineer, laboratory technician and postgraduate students for their contribution to the direction and richness to complete this research.

Besides that, I would like to express my earnest gratitude to my family members and friends who give full support and motivation in achieving my goal. I would like to convey my thanks to Railways Asset Corporation (RAC) and Keretapi Tanah Melayu (KTM) for providing raw material and rail data for complete this research.

Last but not least, my unbounded gratefulness to those who have lent a hand to make this piece of work a success. The thoughtfulness and kind help are much appreciated.

TABLE OF CONTENTS

	PAGE
DECLARATION OF THESIS	i
ACKNOWLEDGMENT	ii
TABLE OF CONTENTS	iii
LIST OF TABLES	vi
LIST OF FIGURES	vii
LIST OF ABBREVIATIONS	xii
LIST OF SYMBOLS	xiii
ABSTRAK	xv
ABSTRACT	xvi
CHAPTER 1 : INTRODUCTION	1
1.1 Background of Study	1
1.2 Problem Statement	3
1.3 Objective	4
1.4 Scope of Study	4
1.5 Thesis Organization	5
CHAPTER 2 : LITERATURE REVIEW	7
2.1 Introduction to Fatigue Crack Initiation	7
2.1.1 Fatigue Crack Growth	8
2.2 Fatigue Constant Amplitude Loading	10
2.3 Linear Fracture Mechanics	12
2.4 Fatigue in Wheel and Rail Rolling Contact	13

2.5	Type of Damages in Rail Profile	14
2.5.1	Rail Corrugation	15
2.5.2	Squats Damages on Railway Rails	21
2.6	Von–Mises Stress Theory of Material	27
2.6.1	Contact Analysis Using Three Dimensional Finite Element Analysis	28
2.7	Head Check Damages on Rail.	30
2.8	Summary	38
CHAPTER 3 : METHODOLOGY		40
3.1	Chapter Overview	40
3.2	Material	42
3.3	Rolling Contact Fatigue	43
3.3.1	Finite Element Analysis Procedure for Study of von–Mises stress	45
3.3.2	Hardness Testing	50
3.4	Specimen Preparation	52
3.5	Dog-bone specimen	53
3.5.1	Fatigue strength Testing Setup	54
3.5.2	Dog-bone Fatigue Analysis Procedure	56
3.6	Compact Tension (CT) Specimen	58
3.6.1	Compact Tension Specimen Precracking Setup	59
3.6.2	Compact Tension Specimen Precracking	61
3.6.3	Fatigue Crack Growth Rate	62
3.7	Summary	66
CHAPTER 4 : RESULTS AND DISCUSSION		68
4.1	Chapter Overview	68
4.2	Rolling Contact Fatigue	68
4.2.1	Vickers Hardness Test	77

4.3	Fatigue S-N Curve	81
4.3.1	Fatigue Strength Analysis	85
4.3.2	Fracture Surface of Dog-bone Specimen	88
4.4	Fatigue Crack Growth Rate	90
4.4.1	Fatigue Crack Growth Rate versus Stress Intensity Range	92
4.4.2	Fracture Surface of Fatigue Crack Growth	99
4.5	Summary	104
CHAPTER 5 : CONCLUSIONS AND RECOMMENDATIONS		106
5.1	Rolling Contact between Wheel and Rail	106
5.2	Fatigue strength of UIC 54 Profile	107
5.3	Fatigue Crack Growth for UIC 54 Profile	108
5.4	Future Work	108
REFERENCES		110
LIST OF PUBLICATIONS		114
APPENDIX A		115
APPENDIX B		116
APPENDIX C		117
APPENDIX D		118
APPENDIX E		119

LIST OF TABLES

NO.		PAGE
Table 2.1:	Mechanical properties of the wheel–rail steel grade 900A (Christodoulou et al. 2016).	13
Table 3.1:	Chemical composition of the rail steel 900A(UIC 54 profile) (in wt. %) (Provided by KTM).	43
Table 3.2:	Convergence testing result for wheel and rail in contact (100 kN).	49
Table 3.3:	Linear material properties for wheel–rail.	50
Table 3.4:	Dog-bone specimen fatigue cyclic loading parameter.	55
Table 4.1:	The result of maximum von–Mises stress between wheel and rail contact.	71
Table 4.2:	Average hardness for new rail (unused condition) at the specified position.	79
Table 4.3:	Average hardness for used rail (failure sample) at the specified position.	79
Table 4.4:	Fatigue strength experimental testing result.	83
Table 4.5:	Material constant value for UIC 54 profile.	99

LIST OF FIGURES

NO.	PAGE
Figure 1.1: Malaysia ETS (KTM, 2017).	1
Figure 2.1: Derailments of Train in Malaysia (KTM BERHAD, 2017)	7
Figure 2.2: Logarithm of the fatigue crack growth rate da/dN versus the logarithm of the stress intensity factor range, ΔK .	8
Figure 2.3: Fatigue constant amplitude loading condition for constant crack growth (Adapted from Anderson, 2005).	11
Figure 2.4: Cyclic loading parameter (test condition, $R = +$) (Budynas, Nisbett, & Shigley, 2011).	11
Figure 2.5: Fatigue crack failure at rail profile (Zerbst et al. 2005).	13
Figure 2.6: Rail head grinding (Grassie et al. 1993).	15
Figure 2.7: Basic feedback loop for rail corrugation mechanism (Adapted from Lewis et al. 2009).	16
Figure 2.8: Heavy-haul corrugation occurred at straight track, high rail of curves. Its happens due to damages mechanism of wear (Adapted from Lewis et al. 2009).	17
Figure 2.9: Heavy-haul corrugation on low rail of the curve on a mixed traffic line. The corrugation form due to plastic flow in troughs (Mair et al. 1977).	18
Figure 2.10: P2 resonance corrugation on a tram system and appeared at straight track or high rail curves with typical. Its happens due to wear damage mechanism at frequency of 50–100. (Grassie et al. 1993).	18
Figure 2.11: P2 resonance and pinned-pinned resonance corrugation at straight track or curves, forms due to plastic bending at frequency of 50–100 (Grassie et al. 1993).	19
Figure 2.12: Rutting corrugation on mainline railways corrugation. This corrugation appeared at low rails of the curves due to wear damage mechanism (Adapted from Lewis et al. 2009).	19
Figure 2.13: Pinned-pinned corrugation on straight track, high rail of the curves. The corrugation was developed due to wear mechanism with typical frequency of 400–1200 (Grassie et al. 1993).	20
Figure 2.14: Corrugation on track with sleepers in resilient boots (trackform-specific corrugation). This corrugation forms due to wear damage mechanism on straight track or curves (Tassilly et al. 1991).	20

Figure 2.15:	Squats damages at different phases of development at top of rail head. The number indicates the length in (mm). (a) Light damage. (b) Moderate damage. (c) Severe damage (Li et al., 2008a).	22
Figure 2.16:	Typical squats damages at weld region. (a) Hardness distribution of thermite and flash butt weld. (b) Hardness different at heat affected zone. (Lewis et al. 2009).	24
Figure 2.17:	Hardness variation at weld region (adapted from Lewis et al. 2009).	25
Figure 2.18:	Geometry variations at weld region (adapted from Lewis et al. 2009).	25
Figure 2.19:	Etched microscopic image for longitudinal direction squats damages for low rail (Steenbergen, 2015).	26
Figure 2.20:	Microscopic image for transverse direction squats (Steenbergen, 2015).	26
Figure 2.21:	General three dimensional stress component for von–Mises model.	28
Figure 2.22:	FEA basic procedure to create a 3D model of rail and wheel	29
Figure 2.23:	3D half symmetry of the rail and the wheel model (Arslan et al. 2012).	29
Figure 2.24:	Contact region between rail and wheel with von–Mises stress gradient (Arslan et al. 2012).	30
Figure 2.25:	Head check damage on rail profile UIC 725 (Popovic et al. 2015).	31
Figure 2.26:	Head check damage at rail steel grade R350HT (Heyder et al. 2014).	32
Figure 2.27:	Material removal and crack propagation at the head of the rail (Heyder et al. 2014).	32
Figure 2.28:	Head check failure at rail profile R350HT (Heyder et al. 2014).	33
Figure 2.29:	Transverse crack propagation at rail profile (Zebrst et al. 2005).	33
Figure 2.30:	Phase of transverse crack propagation starting from head check crack to rail profile root region (final failure) (Zebrst et al. 2005).	34
Figure 2.31:	Head check crack image at 10 MGT for rail profile U75V (Zhou et al. 2014).	34
Figure 2.32:	Head check crack image at 30 MGT for rail profile (Zhou et al. 2014).	35
Figure 2.33:	Head check crack image at 62 MGT for rail profile U75V (Zhou et al. 2014).	35

Figure 2.34:	Head check crack image at 210 MGT for rail profile U75V (Zhou et al. 2014).	35
Figure 2.35:	Sum of the head check crack depth and length for 10MGT, 30 MGT, 62 MGT and 210 MGT (Zhou et al. 2014).	36
Figure 2.36:	U75V profile change to plastic flow and wear due to head check crack million gross ton (MGT). (Zhou et al. 2014).	37
Figure 2.37:	Total traffic load function of the depth of head check growth (R350HT& R250) (Heyder et al. 2014).	37
Figure 3.1:	Flow work of this study.	41
Figure 3.2:	Malaysian High speed rail UIC 54 profile (Provided by RAC).	42
Figure 3.3:	The failure rail sample of UIC 54 (provided by KTM).	44
Figure 3.4:	UIC 54 profile rail model.	44
Figure 3.5:	Model of ETS wheel (diameter 1016 mm).	45
Figure 3.6:	Modelling of the rail and wheel contact in ANSYS Workbench 14.5.	47
Figure 3.7:	3D half wheel and rail assembly model. (a) Full view in contact (b) close view of wheel and rail in contact.	48
Figure 3.8:	Wheel and rail meshed with quadrilateral shapes for element size 1.0 mm.	49
Figure 3.9:	Position of Vickers testing on UIC 54 profile head.	51
Figure 3.10:	Specimen fabrication direction on UIC 54 rail profile.	52
Figure 3.11:	Isometric view of the dog-bone specimen.	53
Figure 3.12:	Seven dog-bone specimen machined from UIC 54 profile head.	54
Figure 3.13:	Dog-bone specimen mounted at 90° onto Instron 8800.	55
Figure 3.14:	Geometry of dog-bone model imported from Catia software.	57
Figure 3.15:	Dog-bone meshed with quadrilateral shapes for element size 0.3 mm.	57
Figure 3.16:	Isometric view of compact tension specimen.	58
Figure 3.17:	The configuration of compact tension specimen (ASTM E 647–15).	59
Figure 3.18:	Precracking test set up on Instron 8800 100kN fatigue test machine.	60
Figure 3.19:	Reference plane for precracking (ASTM E 647–15).	60

Figure 3.20:	Precracking length against a number of the cycle for all CT specimen.	61
Figure 3.21:	Crack propagation at CT specimen notch during precracking.	62
Figure 3.22:	Finished compact tension specimen from the web of UIC 54 profile (Transverse direction).	63
Figure 3.23:	Instron 8800 100 kN fatigue testing machine.	64
Figure 3.24:	CT specimen mounted into Instron 8800 machine with clevis and pin assembly.	64
Figure 4.1:	Full model of wheel and rail (von-Mises stress) in static loading for 100 kN vertical loading.	69
Figure 4.2:	Full model of wheel and rail (von-Mises strain) in static loading for 100 kN vertical loading.	70
Figure 4.3:	Stress gradient distribution at rail gauge corner region due to contact between wheel and rail.	72
Figure 4.4:	Stress gradient at rail head for 80 kN vertical loading.	73
Figure 4.5:	Stress gradient at rail head for 90 kN vertical loading.	73
Figure 4.6:	Stress gradient at rail head for 100 kN vertical loading.	74
Figure 4.7:	Stress gradient at rail head for 110 kN vertical loading.	74
Figure 4.8:	Stress gradient at rail head for 120 kN vertical loading.	75
Figure 4.9:	Maximum stress concentration at rail gauge corner from for all tested vertical loading (80 kN to 120 kN).	76
Figure 4.10:	Vickers Hardness testing result for new rail (unused condition) versus used rail (failure sample).	80
Figure 4.11:	Maximum hardening region at rail inside curve (shaded line A) P1 to P3.	80
Figure 4.12:	Fatigue S-N curve of UIC 54 profile (grade 900A).	83
Figure 4.13:	Dog-bone specimen after Fatigue strength testing. (a) 16.7% (b) 25% (c) 35% (d) 50%.	84
Figure 4.14:	Dog-bone specimen after Fatigue strength testing. (e) 58.35 (f) 66.7% and (g) 76%.	84
Figure 4.15:	Fatigue strength gradient for 50% stress level.	85
Figure 4.16:	Fatigue strength gradient for 58.3% stress level.	86

Figure 4.17:	Fatigue strength gradient for 66.7% stress level.	86
Figure 4.18:	Fatigue strength gradient for 75% stress level.	87
Figure 4.19:	Fatigue strength S–N for Fatigue analysis and experimental.	88
Figure 4.20:	SEM picture of different region on fractured surface UIC 54 profile for 66.7% stress level.	89
Figure 4.21:	Fatigue crack growth for all CT specimens.	91
Figure 4.22:	Failure CT specimen 1 at 16 kN, $R = 0.1$.	92
Figure 4.23:	Fatigue crack growth rate for all specimen with ESDU 81011 fatigue crack growth propagation data.	94
Figure 4.24:	Linear region of da/dN vs. ΔK plot of specimen 1.	96
Figure 4.25:	Linear region of da/dN vs. ΔK plot of specimen 2.	97
Figure 4.26:	Linear region of da/dN vs. ΔK plot of specimen 3.	98
Figure 4.27:	The sectional view of failure surface (16kN, $R = 0.1$).	100
Figure 4.28:	Region A (16 kN, $R = 0.1$).	100
Figure 4.29:	Region B (16 kN, $R = 0.1$).	101
Figure 4.30:	Region C (16 kN, $R = 0.1$).	101
Figure 4.31:	The sectional view of failure surface (Specimen 3).	102
Figure 4.32:	Region A (13 kN, $R = 0.1$).	102
Figure 4.33:	Region B (13 kN, $R = 0.1$).	103
Figure 4.34:	Region C (13 kN, $R = 0.1$).	103

LIST OF ABBREVIATIONS

ASTM	American Society for Testing and Materials
CT	Compact tension
ETS	Electric train service
EDM	Electrical discharge machining
FEA	Finite element analysis
FCGR	Fatigue crack growth rate
UIC	International Union of Railways
KTM	Keretapi Tanah Melayu
MGT	Million gross ton
RAC	Railway Assets Corporation
RCF	Rolling contact fatigue
UTS	Ultimate tensile strength
SEM	Scanning electron microscope
SIF	Stress Intensity Factor

©This item is protected by original copyright

LIST OF SYMBOLS

a	Crack length (after Precracking)
a_n	Notch length (initial crack length)
A	Specimen area
B	Specimen thickness
C, m	Fit parameters of the $da/dN-\Delta K$ curve in the Paris range
da/dN	Fatigue crack propagation rate
E	Modulus of elasticity
f	Frequency of cyclic loading
HV	Vickers hardness
K	Stress intensity factor
K_{max}	Maximum stress intensity factor
K_{min}	Minimum stress intensity factor
N	Number of loading cycles
ΔP	Applied load Range
P_{max}	Maximum applied load
P_{min}	Minimum applied load
R	R stress ratio ($\sigma_{min} / \sigma_{max}$)
W	Specimen width
K_{IC}	Critical stress intensity range
ΔK_{th}	fatigue crack propagation threshold
σ_a	Stress amplitude
σ_m	Mean stress
σ_{max}	Maximum stress in the fatigue cycle
σ_{min}	Minimum stress in the fatigue cycle
σ_{UTS}	Ultimate tensile strength

σ_y Yield strength

©This item is protected by original copyright

Siasatan Kadar Perambatan Retak Lesu pada profil UIC 54 Dalam Aplikasi Landasan Berkelajuan Tinggi

ABSTRAK

Keselamatan roda dan landasan keretapi adalah merupakan kebimbangan yang besar bagi sektor Keretapi Tanah Melayu dan pengeluar rangkaian keretapi. Pengegekan sentuh lesu (RCF) adalah masalah yang semakin meningkat disebabkan oleh peningkatan operasi kereta api berkelajuan tinggi di Malaysia dan peningkatan kitaran pembebanan oleh putaran roda atas landasan. Retak biasa yang berasal daripada permukaan landasan keretapi disebut sebagai semakan turus manakala, retakan melintang membawa kepada kegagalan fungsi landasan keretapi disebabkan perambatan retak yang terlalu cepat pada landasan keretapi. Dalam kajian ini, analisis berangka pada tegasan-terikan tiga dimensi (3D) bagi roda kereta api berjaya dijalankan oleh ANSYS Workbench 14.5. Kajian ini lebih tertumpu kepada eksperimen, kekuatan hayat lesu dan kadar pertumbuhan retakan (FCG) daripada UIC 54 profil kereta api. Kekuatan hayat lesu dan kajian FCG telah diselaraskan dengan spesimen pukal (ASTM E-466-15), dan tegangan padat (CT) spesimen (ASTM E-647-15). Lekuk S-N telah diplotkan daripada 7 set data spesimen pukal untuk menilai kekuatan lesu hayat dengan kadar nisbah pemalar boleh ubah pada tegasan 0.1. Di samping itu, profil UIC 54 lesu hayat telah disahkan dengan keputusan simulasi menggunakan ANSYS Workbench 14.5. Kerja-kerja simulasi telah dilaksanakan dengan spesimen model pukal mengikut tahap tegasan kenaaan eksperimen. Selain daripada itu, kajian FCG itu dijalankan dengan menggunakan CT spesimen dengan pemboleh ubah dalam nisbah tegasan sebanyak 0.1, 0.3 dan beban 16 kN dan 13 kN digunakan. Kadar pertumbuhan retak bahan untuk profil UIC 54 diperolehi dari hubungan C dan m Paris-Erdogan. Hasil tegasan von-Mises menunjukkan bahawa zon tumpuan tegasan maksimum telah dicapai pada tolok kereta api di setiap sudut penjuru melebihi had kekuatan alah (533 MPa). Tambahan pula, hasil tegasan plastik yang setara menunjukkan bahawa kebanyakan ubah bentuk plastik berlaku di sudut penjuru landasan. Pengukuran kekerasan keseluruhan untuk landasan yang digunakan memperoleh 37.9 % lebih besar daripada landasan yang tidak digunakan. Nilai kekerasan untuk P1 (landasan yang digunakan) menunjukkan bahawa sudut penjuru landasan terjejas oleh tegasan hubungan tinggi dan ricihan plastik. Hasil ujian kekuatan lesu untuk profil UIC 54 ditunjukkan dalam trend dimana bilangan kitaran lesu adalah lebih kecil dengan amplitud tekanan tinggi. Melalui lekuk S-N, had ketahanan diperolehi untuk profil UIC 54. Di samping itu, had ketahanan telah disahkan daripada hasil simulasi kekuatan lesu. Daripada penemuan ini, rintangan pertumbuhan retak lesu adalah kurang untuk profil UIC 54, yang telah diperolehi dari nilai tinggi parameter pertumbuhan retak lesu m untuk spesimen 1 ($m = 3.455$), spesimen 2 ($m = 3.270$) dan spesimen 3 ($m = 3.223$). Analisis mesin imbasan elektron (SEM) untuk spesimen pukal dan spesimen tegangan padat telah dilakukan di permukaan patah. Daripada pemerhatian keputusan analisis ini, permukaan patah telah mengalami kegagalan retak lesu yang tinggi pada jangka hayat bagi profil UIC 54. Hasil eksperimen kekuatan hayat lesu akan menjadi signifikan bagi landasan keretapi untuk memilih profil kekuatan hayat lesu yang tinggi dan untuk mengira jangka hayat profil UIC 54. Nilai malar C dan m digunakan untuk mengira kadar pertumbuhan retak melintang untuk profil UIC 54 dan untuk mengelakkan kegagalan dan kerosakan landasan semasa beroperasi. Kajian FCG boleh dijalankan dengan beban muatan mampatan untuk menyiasat mod retak di rantau retak dengan nisbah tegasan, $R = -1$.

An Investigation of Fatigue Crack Growth Behavior of UIC 54 Profile in High Speed Railway Applications

ABSTRACT

The safety of wheels and rails is a greater concern for the Malaysian railways Keretapi Tanah Melayu and manufacturers of the railway network. The rolling contact fatigue (RCF) is a growing problem due to increase of the high speed train operation in Malaysia and increased of load cycle. The RCF is defined as a damage that occurred due to the change in the material microstructure which contributes to crack initiation followed by crack propagation under the influence of time-dependent. The typical cracks originating at the running surface is called as head check. The transverse cracks leading to the eventual fracture of the rail. As well as the crack growth rate is higher, it caused the crack to propagate faster and initiate the sudden rail failure at any time. In this study, numerical analysis of stress-strain characteristics of three dimensional (3D) wheel-rail contact was successfully carried out by ANSYS Workbench 14.5. Apart from that, this study focuses on the fatigue strength and fatigue crack growth (FCG) of UIC 54 profile. The fatigue strength and FCG study were coordinated with the dog-bone specimen (ASTM E-466-15) and compact tension (CT) specimen (ASTM E-647-15), respectively. The S-N curve was plotted from 7 data of the dog-bone specimens to evaluate fatigue strength with a constant stress ratio 0.1, and variable in applied stress levels. In addition, the rail profile of UIC 54 fatigue strength was validated with simulation result by ANSYS Workbench 14.5. The simulation works were executed with dog-bone specimen model according to the experimental applied stress level. Meanwhile for FCG the study was conducted with the CT specimens with a variable in stress ratio of 0.1, 0.3 and applied loads of 16 kN and 13 kN. The material crack growth rate for UIC 54 profile is obtained from Paris-Erdogan relationship C and m . The maximum von-Mises stress result for the wheel and rail contact was obtained higher at rail gauge corner region and it's exceed the yield strength limit (533 MPa) of UIC 54 profile. Furthermore, the equivalent plastic stress result reveals that most of the plastic deformation occurs at the rail gauge corner region, on the contrary almost very small plastic deformation occurs at the wheel. The overall hardness measurement for used rail obtained was 37.9 % greater than unused rail. The hardness value for P1 (used rail) indicates that rail gauge corner region was affected by high contact stresses and plastic strains. The result of fatigue strength testing for UIC 54 profile was shown as in the trend, i.e. at the smaller number of fatigue cycle with high stress amplitude. From the S-N curve results, the endurance limit was obtained for UIC 54 profile. In addition, the endurance limit was validated from simulation results fatigue strength. From the finding, the fatigue crack growth resistance is poor for UIC 54 profile, characterized by a high value of crack growth rate parameter m for specimen 1 ($m = 3.455$), specimen 2 ($m = 3.270$) and specimen 3 ($m = 3.223$), respectively. The scanning electron microscope (SEM) observation at the dog-bone specimen and CT specimen on fracture surface was conducted. The fatigue strength experimental result will be significant for Malaysian Railways for selecting the high fatigue strength profile and to calculate the lifespan of UIC 54 profile. The constant value of C and m used to calculate the transverse crack growth rate for UIC 54 profile and to prevent from the rail failure and breakdown during its service time. In advance of that, the FCG study can be conduct with compression loading stress to investigate on the mode of fracture at the crack region with stress ratio of, $R = -1$.

CHAPTER 1 : INTRODUCTION

1.1 Background of Study

Today in Malaysia, the railway is one of the public transportation as it offers safety, comfort and speed. According to F.M.S.Railway (2017), “Keretapi Tanah Melayu” (KTM) was established 55 years ago and initially known as “Keretapi Tanah Melayu Berhad” (KTMB). In Malaysia, the high speed train is operational since year 2010 as shown in Figure 1.1. On July 2015, the Electric Train Service (ETS) was started to operate from north Malaysia to Sentral Kuala Lumpur and by the year 2024 this services will be extended to east coast region of Malaysia.



Figure 1.1: Malaysia ETS (KTM, 2017).

On the other hand, the annual passenger statistics shows 56% increment from the year 2015 to 2016 for ETS as in Appendix A. Therefore, the railway tracks in

Malaysia has to be improved in safety and reliability to withstand the repeated cyclic loading. In addition, the wheel and rail are main components of railways system, for that the initial damages from wheel and rail contact have to be identified in order to take precaution on the Malaysia railway system. Smith (2009), reported that the fatigue failure causes in many components in different industries and until now the problem still exists in railways. Moreover, the increase in train performances and rail traffic necessitate the development of good damage tolerance material to support the KTM. The damage may occur due to the rolling contact fatigue (RCF) and is one of the main factor influencing to growth of fatigue problems in railways. The fatigue performance of the rails is affected by many factors, including service conditions, loading, mechanical properties, environment factors, and manufacturing processes as reported by Arslan et al. (2012). RCF is defined as a damage because of change in the material microstructure which contributes to crack initiation followed by crack propagation, under the influence of time-dependent rolling and sliding contact loads.

The RCF in rail is caused by the wheel–rail contact which leads to initiation of surface and subsurface cracks as stated Masoudi et al. (2016). Reis et al. (2014), investigated that the main reason of RCF occurs is due to the operation increased on high speed railways and increased number of loading cycle between wheel–rail contact region. In this present study, the RCF failure analysis was executed by using ANSYS finite element software. The common problem which identifies from the failure of wheel and rail such as side wear, fatigue crack, crushing, corrugation and etc. Apart from that, this investigations focuses on fatigue strength and fatigue crack growth (FCG) of Malaysia High speed train UIC 54 profile.

1.2 Problem Statement

Damage accumulation due to fatigue, plastic deformation and wear, significantly reduces the life service of life in the railway system. In recent years, the increase in train speeds (high speed train) leads to larger wheel–rail contact forces. These failures may cause damages to rails, train suspensions and in rare cases may occur serious derailment/slip of the train. The fatigue problem of wheel–rail is often referred to as RCF, which is caused by repeated contact stress during the rolling motion. Furthermore, the RCF between the wheel and the rail is generated the contact stress in form of elastic or plastic at the material. The contact stresses can be superimposed by residual stresses, normal stresses due to bending of the axle or thermal stresses, resulting in a complex stress state at the tip of a growing crack. Depending on the resulting stress state and the railway material, the surface crack will propagate and may branch downwards toward the body of the rail, usually under combined mode I/II loading. If left untreated the crack length can become critical, endangering the structural integrity of the rail. Furthermore, RCF is defined as a damage that occurred due to the change in the material microstructure which contributes to crack initiation followed by crack propagation under the influence of time-dependent. Moreover, the rail profile appears small surface fatigue cracks due to large contact stress. The growth and connection of surface fatigue cracks would result in the material removed from rail surface and then this leads to serious damages of railway system. The typical cracks originating at the running surface is called as head check. The transverse cracks leading to the eventual fracture of the rail. As well as the crack growth rate is higher, it caused the crack to propagate faster and initiate the sudden rail failure at any time.

1.3 Objective

- a) To analyse the damaged sample given by KTM on the effect of rolling contact fatigue (RCF) between wheel and rail contact region by using finite element analysis (FEA).
- b) To determine the fatigue strength of UIC 54 profile at the head region with dog-bone specimen.
- c) To evaluate the fatigue crack growth rate (FCGR) of UIC 54 profile at web region with compact tension (CT) specimen.

1.4 Scope of Study

The scope of the study is to investigate the fatigue strength and fatigue crack growth of railway rail steel grade 900A International Union of Railways (UIC 54) profile. The UIC 54 profile has been used to manufacture the rail by Malaysian railway for several decades. The 3D finite elements analysis is performed between wheel and rail to analysis maximum stress field distribution at rail inside curve region. Apart from that, the hardness measurements testing on UIC 54 profile at used and unused rail profile head. Furthermore, the hardness testing is conduct according to ASTM E 92-16 Standards. The dog-bone specimen and CT specimen experimental setup and testing are conducted according to ASTM E 466-15 and ASTM E 647-15 Standard, respectively. The fatigue strength (S-N) curve is plotted using seven dog-bone specimens with variable stress amplitude and with constant stress ratio of 0.1. Besides that, FCGR investigation, (da/dN versus ΔK) testing is conducted with CT specimen on constant machine frequency of 20

Hz and variable in applied loads of 13 kN and 16 kN. The testing stress ratio, R for FCGR testing is set 0.1 and 0.3 to investigate the effect of stress ratio of UIC 54 profile.

1.5 Thesis Organization

The thesis is divided into five chapters. In general, the first chapter describes about the introduction, problem statement, objectives and scopes of study. The aim of this chapter to explain briefly about the importance of this research to the readers.

Chapter 2 contains literature review which collected from others researcher with the same field of study. Furthermore, this chapter is also included with theories and background study about RCF, fatigue behavior of rail steel, rail damages, head check at rail inside curve and transverse crack at rail profile that have been taken into consideration.

Chapter 3 is research methodology which explained the simulation and experimental process. Moreover, this chapter represents about details on material properties and methods to conduct this study. The simulation part was created based on damage sample and data given by KTM. Furthermore, the experimental testing and simulation analysis is conducted with the dog-bone specimen/model to determine the fatigue strength for UIC 54 rail profile. Meanwhile, the FCGR result was obtained from da/dN vs. ΔK data.

Chapter 4 consist of results and discussion of the final results. In this chapter the final results obtained from simulation and experimental data were compiled and

discussed as well. The 3D finite element model is used to investigate the effect of RCF between wheel and rail head region. Apart from that, the data from fatigue testing machine (Instron 8800) are collected and recorded from S-N curve and FCGR results for rail profile UIC 54.

Chapter 5 provides the conclusion for this research. In this chapter, the final conclusion of the study is discussed by referred to the simulation and experimental results. There is also discussion about the further works and recommendation that can be applied to this study.

©This item is protected by original copyright

CHAPTER 2 : LITERATURE REVIEW

2.1 Introduction to Fatigue Crack Initiation

According to Ringsberg et al. (2001), the life of a fatigue crack is divided into 3 phases. Phase I is about the shear stress applied to the surface which was initiated the crack, phase II is the transient crack growth behavior and phase III is the subsequent tensile and shear driven crack growth. The engineering structure deterioration due to fatigue has been a major issue faced by engineers. Akeel et al. (2011) reported that the estimated fatigue failure is more than 70% in engineering structure and this leads researchers to investigate on crack propagation, crack path and stress intensity factor as shown in Figure 2.1.



Figure 2.1: Derailments of Train in Malaysia (KTM BERHAD, 2017)

2.1.1 Fatigue Crack Growth

The fatigue crack growth studies are conducted by many researchers with dynamic loading. There are various studies on fatigue behavior based on rail profile types as stated by Grassie et al. (1993). However, there is a number of controversial problems and unanswered question in those studies. Paris et al. (1963), presented that the fracture mechanics are one of the tools to study the fatigue crack growth in metals. In general, FCGR curve is conducted in semi or wholly empirical manner. The researchers widely used the Paris law which is published in Paris et al. (1961). Figure 2.2 is a schematic log-log plot da/dN versus ΔK , which illustrates typical fatigue crack growth behavior in the metallic material. Anderson (2005), stated that the sigmoidal curve consists of the three distinct regions and a linear region of the log-log plot that can be described by the power law in Equation 2.1

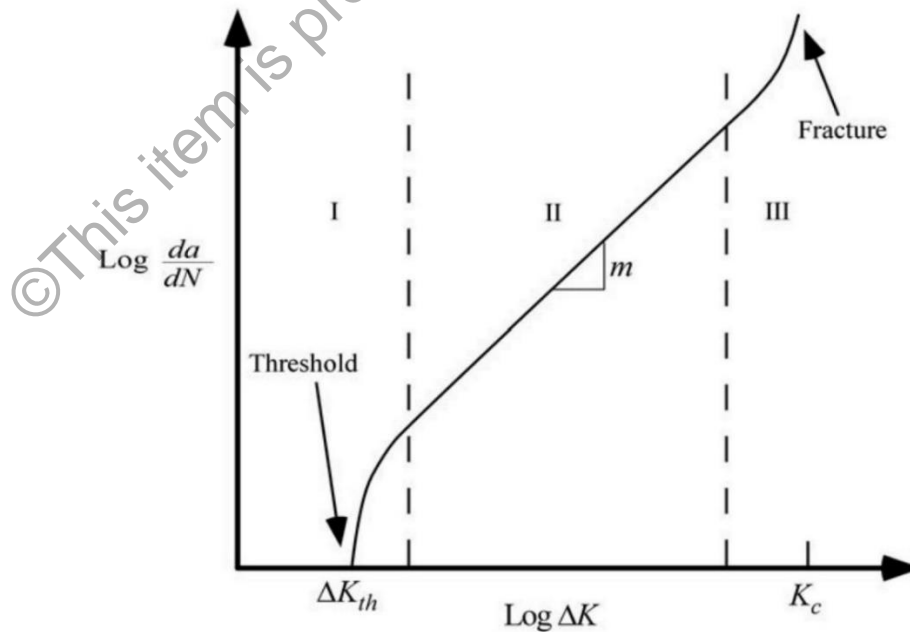


Figure 2.2: Logarithm of the fatigue crack growth rate da/dN versus the logarithm of the stress intensity factor range, ΔK .